Using Raman Spectroscopy to study Supercritical CO_2

by

Pankaj Bhatia

MSc (Integrated), Chemistry
Indian Institute of Technology, Kanpur, 1997

Submitted to the Department of Chemistry
in partial fulfillment of the requirements for the degree of

Master of Science (SM) in Chemistry

at the

MASSACHUSETTS INSTITUTE OF TECHNOLOGY

June 1999

Author.....

Department of Chemistry,
May 2nd, 1999

Certified by.....

Prof. Jeffrey Irwin Steinfeld
Department of Chemistry
Thesis Supervisor

Accepted by.....

Dietmar Seyferth
Chairman, Departmental Committee on Graduate Studies

To,
My family for their constant support and inspiration.....

Using Raman Spectroscopy to study Supercritical CO_2

by

Pankaj Bhatia

Submitted to the Department of Chemistry
on May 2nd, 1999 in partial fulfillment of the requirements
for the degree of Master of Science (SM)
in Chemistry

Thesis Supervisor: Professor Jeffrey I Steinfeld

Abstract

We have measured the Raman active modes of CO_2 starting from below the critical point at 800 psi or 55 bars and 23.5 °C through the critical point upto 1500 psi or 103 bars and 41.4 °C. It is shown that the Intensity of the symmetric stretch band at 1388 cm^{-1} increases with density. No significant changes are observed in the band shapes and the width of the Raman bands do not change at all as a function of T and P. It is thus obvious that the width or Full Width at Half Maxima (FWHM) is not a good parameter for Molecular Modeling. Moreover, it is also experimentally shown that the band at 1500 psi and 41.4 °C above the supercritical conditions shows a small blue shift relative to the bands at lower T and P conditions. Even though it is implied that CO_2 does not change significantly in its molecular geometry, it is clear that molecular dynamics calculations are needed to relate the band shapes to the phase changes from a liquid to a vapor phase to a supercritical phase. Also, it is agreed that the local density enhancememts can be better studied by putting a solute in CO_2 solvent. This study is an attempt in the direction of modeling insitu organic reactions using Raman spectroscopy and designing environmentally benign chemical processes by replacing organic solvents with CO_2.

Acknowledgements

I would like to thank my advisor, Prof. Jeffrey I Steinfeld for his patience and guidance during my graduate research at MIT. I would also like to thank Prof. Robert Field for his guidance while I struggled to find a place in the department.

All the members in the group, past and present, have been very helpful and friendly and I would like to thank them for their friendship and help. They are Arturo Casielles, Markus Haider, Joshua Taylor, Matt Gardner, Scott Witonsky, Shangfu and Manjula. I would especially like to thank people who have worked with me on the Raman project especially Arturo, Markus and Josh and taught me about Raman spectroscopy and supercritical fluids. Also, appreciate everyone's patience while working with me on the project, around the laboratory and for being kind enough to answer my questions on spectroscopy, in general.

Special thanks to my advisor, Jeff for his patience and constant support and his approval in allowing me to work in the summers at Molecular Simulations Inc. in San Diego.

Of course, thanks to my good friends at MIT, Sudipta and Evan for caring and patient with me. Thanks for their friendship, thanks for comforting me in times of trouble and making made my stay at MIT memorable and joyful.

I also thank Balaji for giving me the strength and the motivation to come to MIT and work hard. MIT is a great school and I feel fortunate to be a part of a great institution. Even though I feel I have learnt a lot during the past two years, I also feel that life is a constant learning process. Personally, I feel proud to graduate from a great school.

Most importantly, I would like to thank my family and my brother, Kamal for their unconditional and unflagging support in both good times as well as bad. This thesis would not have been possible without any of you. Thank you all.

Table of Contents

Abstract **3**

I. Introduction **6**

II. Theory **11**
A. Overview of Raman Spectroscopy.....11
B. Relation between Raman Band Shapes and potential.....13

III. Experimental Setup and Measurement
A. Design of High P, High T Raman system.....21
B. Measurement.....22
C. Computer Interface for Data Acquisition.....24

IV. Results and Interpretation
A. Temperature dependence.....27
B. Pressure dependence.....30

V. Conclusion **35**

I. INTRODUCTION:

Every stable compound has a triple and a critical point. Any gaseous compound becomes supercritical when compressed to a pressure higher than the critical pressure ($\mathbf{P_c}$) above the critical temperature ($\mathbf{T_c}$). Properties of supercritical fluids (SCFs) are different from those of ordinary gases and liquids and are tunable simply by changing the pressure and temperature. In particular, density and viscosity change drastically at conditions close to the critical point. The solvating power is much smaller than that of conventional fluid solvents but this can be utilized to generate unique molecular clusters or assemblies in a homogenous phase. This way the SCFs offer a potential opportunity to tune density and intramolecular interactions between a solute and a solvent. Such phenomena have been recognized in spectroscopic studies[1), 2)], and the same effects are expected to change chemical reactivity and selectivity.

SCFs also offer technical advantages and their characteristics have been exploited in chromatography and chemical processes, particularly in a variety of extraction and separation processes, and also as reaction media. They form a single-phase mixture with gaseous reactants, sometimes avoiding a rate limiting mass transfer step and thus enhancing reaction rates. Currently, large-scale chemical manufacturing is facing a serious problem in connection with organic solvents. Regulation of the use of hazardous organic solvents such as chlorinated hydrocarbons is becoming increasingly stringent and spurs the development of environmentally benign, economical reaction media.

Supercritical carbon dioxide ($SCCO_2$) is readily accessible with a T_c of 31°C and a P_c of 73 bar or 1095 psi (see Fig.1), and has excellent potential

for being used as a substitute for environmentally unacceptable solvents. It is abundant, inexpensive, nonflammable, nontoxic and environmentally benign. It has a high solubility for nonpolar organic compounds. Although its ability to dissolve polar, ionic or polymeric compounds is exceedingly limited, small amounts of a polar additive or an appropriate surfactant dramatically change the microenvironment to greatly increase the solubility of such substances. Perfluorinated compounds are particularly effective for this purpose, expanding greatly the applicability of CO_2[3]. Since the use of $SCCO_2$ allows facile separation of reactants, catalysis and products, it may eventually be used as a substitute for environmentally less acceptable solvents. In connection with "green" technology, water is another likely SCF medium. Surprisingly, unlike ambient liquid water, supercritical water is relatively nonpolar but highly acidic, although it requires harsh conditions (T_c = 374 °C and P_c = 218 bar). This phase can be used to decompose chemical wastes. Thus, SCFs such as supercritical water (SCW) have been used for the complete destruction of toxic wastes. It would thus appear that SCW is a promising media for a wide range of thermochemical reactions including reduction, pyrolytic and dehydration reactions.[4), 5)] Also applications for $SCCO_2$ have been found in the extraction [6), 7)], separation and chemical reactions in the food processing and the chemical industries.

On one hand, extensive efforts are being made to find technological applications of SCW and $SCCO_2$ as well as for putting results of application development into practical use. On the other hand, there have been few studies considering SCW and $SCCO_2$ from a fundamental point of view. As reported in studies on phenomena in $SCCO_2$ [8), 9), 10), 11)], the reaction rate and selectivity in the vicinity of the critical point seem to be influenced by changes in the association effect acting between reactants, changes in solvation, and rearrangement of the solvent molecules. It is thus necessary to efficiently control reactivity of decomposition and recombination in $SCCO_2$ as a reaction medium. For the same reason, it is

also extremely important to study supercritical solution chemistry at the molecular level through spectroscopic experiments, including the clarification of the structure of $SCCO_2$ as a reaction medium and further the investigation on how the solvent characteristics of $SCCO_2$ influence the chemical reactivity and the active complex structure. In chemical reaction kinetics, attempts have been made to increase reaction rates drastically and to develop new reaction mechanisms utilizing changes in fluid density by controlling T and P.[12), 13)]

The microscopic structure of a solution is reflected in macroscopic physicochemical characteristics, such as boiling point, melting point and dielectric constant. The best ways to clarify microscopic factors involved in SCFs are experimental verification, including study of solution structures by x-ray and neutron diffraction methods[14)], studying of dynamics mainly by NMR[15)], and studying of vibrational spectra by Infrared, Raman spectroscopy or similar methods. These methods, however, involve difficulties because it is necessary to establish *in situ* measurements under high T, high P conditions. Laser Raman spectroscopy obviates many of the problems associated with other analytical techniques and helps obtain direct information on molecular symmetry in gaseous and critical phase through frequency shifts and depolarization ratio because the measurement is conducted through a scattering of the incident photons[16), 17)]

In this study, we attempt to show that the information provided through molecular models established via line shape analysis of Raman bands can be useful for understanding the underlying enigma behind $SCCO_2$ and its physicochemical properties. We also present any inferences that we can from the above study.

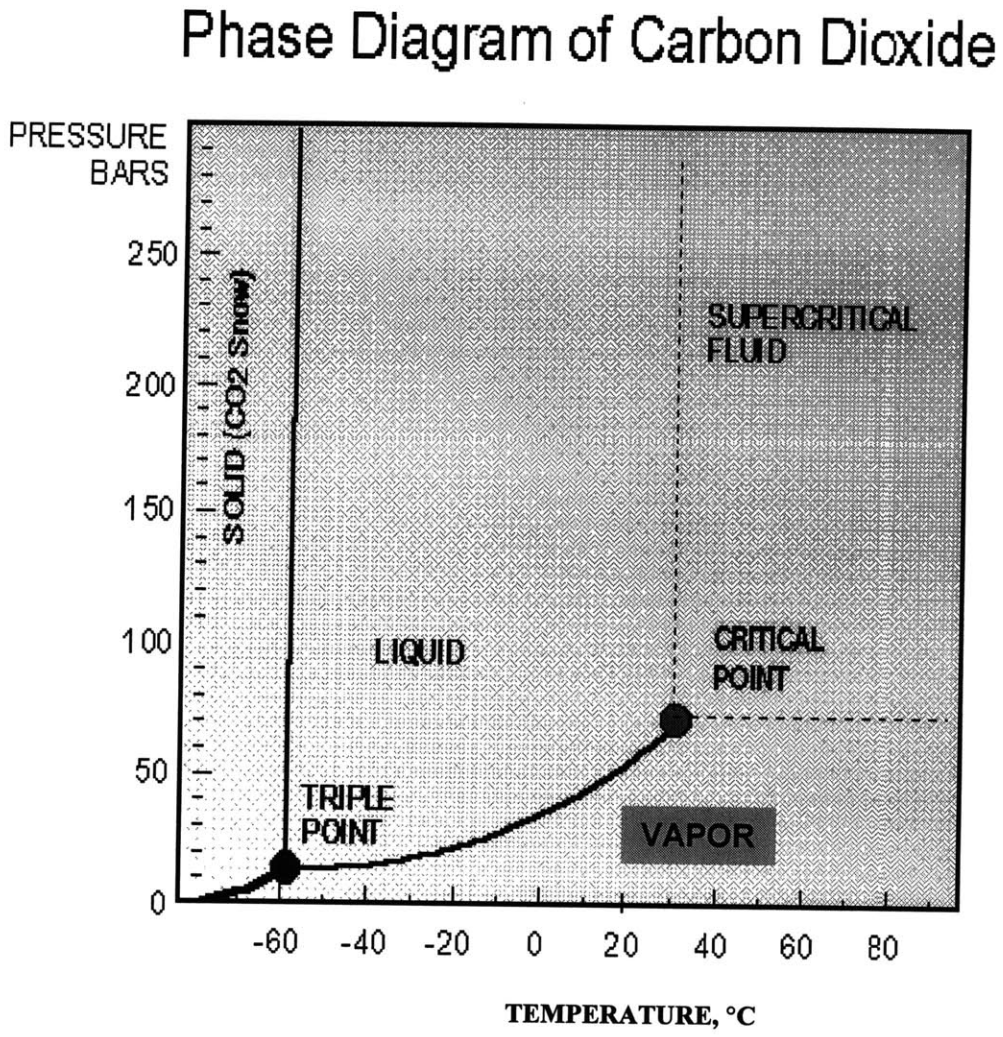

Fig.1: Phase diagram of Carbon dioxide (CO_2) illustrating the critical conditions at $T_c = 31°C$ and $P_c = 73$ bar (1 bar = 14.583 psi)

II. THEORY:

A. Overview of Raman Spectroscopy:

The Raman effect is light scattering following excitation by the incident light. The scattered light consists of two types: **Rayleigh scattering**, which is strong and of the same frequency as the incident light (ω_o) and Raman scattering which is typically, very weak (10^{-5} the intensity of the incident beam) with frequencies $\omega_o+\omega_m$ **(anti stokes)** and $\omega_o-\omega_m$ **(stokes)** where ω_m is the vibrational frequency of the molecule.

The origin of the Raman effect may be derived classically. The electric field strength fluctuates in time, $E= E_o\cos\omega_o t$ where E_o is the field amplitude and ω_o is the frequency of the incident light (usually a monochromatic laser is employed).

The induced dipole moment is thus:

$\mu_{ind} = P = \alpha . E = \alpha E_o \cos\omega_o t$ where α is the polarizability tensor.

Components in **x, y and z** are:

$$P_x = \alpha_{xx}E_x + \alpha_{xy}E_y + \alpha_{xz}E_z$$

$$P_y = \alpha_{yx}E_x + \alpha_{yy}E_y + \alpha_{yz}E_z$$

$$P_z = \alpha_{zx}E_x + \alpha_{zy}E_y + \alpha_{zz}E_z$$

If the molecule is vibrating with frequency ω_m , the displacement **q** is described as $\mathbf{q} = \mathbf{q_o}\cos\omega_m t$. Expanding the polarizability tensor in Taylor series in the normal coordinates of vibration, evaluated at equilibrium is:

$$\alpha = \alpha_o + (\partial\alpha/\partial q)_o q + \tfrac{1}{2}(\partial^2\alpha/\partial q^2)_o q^2 + \textit{higher order terms}$$

Ignoring powers of q higher than the first (sometimes referred to as the electrical harmonic approximation),

$$P = \mu_{ind} = \alpha_o E_o \cos\omega_o t + (\partial\alpha/\partial q)_o q_o \cos\omega_m t \, (E_o \cos\omega_o t)$$

But $\cos A \cos B = \frac{1}{2}[\cos(A+B)+\cos(A-B)]$, so

$$\mathbf{P = \mu_{ind} = \alpha_o E_o \cos\omega_o t + (\partial\alpha/\partial q)_o E_o q_o \tfrac{1}{2}[\cos(\omega_o+\omega_m)t + \cos(\omega_o-\omega_m)t)]}$$

Thus the overall contribution to polarization is from Rayleigh scattering (ω_o), antistokes ($\omega_o + \omega_m$) and stokes ($\omega_o - \omega_m$), as shown in Fig.2 below.

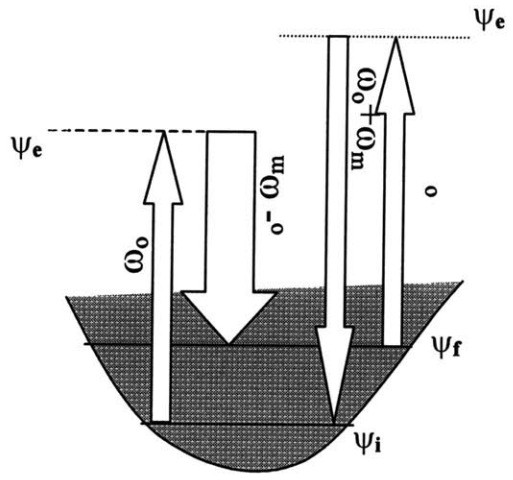

Fig. 2: A pictorial representation of the Raman experiment

The antistokes scattering is much less than stokes owing to the population differences between v = 0 and v = 1(higher vibrational level).
The Raman intensity can be shown to be:

$$\mathbf{I_{i\to f} = cI_o(\nu_o - \nu_{if})^4 \Sigma_{\rho\sigma} |(\alpha_{\rho\sigma})_{if}|^2}$$

where **i** and **f** denote the initial and final vibrational states, respectively of the electronic ground state. The change in polarizability α, caused by the

i→e→f transition for the ρ and σ **x, y and z** components of the polarizability tensor is:

$$(\alpha_{\rho\sigma})_{if} = \mathbf{1/h} \sum_e (\langle \mathbf{i} \mid \mu_\rho \cdot \varepsilon \mid \mathbf{e} \rangle \langle \mathbf{e} \mid \mu_\rho \cdot \varepsilon \mid \mathbf{f} \rangle / (\nu_{ei} - \nu_o + i\Gamma_e)) \quad +$$

$$(\langle \mathbf{i} \mid \mu_\rho \cdot \varepsilon \mid \mathbf{e} \rangle \langle \mathbf{e} \mid \mu_\rho \cdot \varepsilon \mid \mathbf{f} \rangle / (\nu_{ef} + \nu_o + i\Gamma_e))$$

where e represents an electronic or virtual excited state and consequently ν_{ei} and ν_{ef} are the frequency differences corresponding to the energy differences between the states. Γ_e is the bandwidth of the e^{th} state. In normal Raman scattering $\nu_o << \nu_{ei}$.....namely the energy of the incident beam is less than the electronic transitions. In this case the Raman intensity is proportional to $(\nu_o - \nu_{if})^4$.

More generally the Raman intensity depends on the change in polarizability upon excitation. If there is no change i.e., $(\alpha_{\rho\sigma})_{if} = \mathbf{0}$, the transition is forbidden. With regard to the above expression, the product integrals, $\langle \mathbf{i} | \mu_\rho \cdot \varepsilon | \mathbf{e} \rangle \langle \mathbf{e} | \mu_\sigma \cdot \varepsilon | \mathbf{f} \rangle$ must exhibit transformation properties that contain the totally **symmetric** representation. The operator transforms as the product $\mu_\rho \cdot \mu_\sigma(\rho\sigma)$ where ρ,σ = x, y, z which has the form of a binary product.

The overall form of the transformation properties of the transition moment integral for scattering thus becomes:

$$\Gamma(\Psi^f_{vib}) \otimes \Gamma(\alpha_{\rho\sigma}) \otimes \Gamma(\Psi^i_{vib})$$

But $\Psi^f_{vib} \approx H_v(\sqrt{\alpha_q})$; $\Psi^i_{vib} \approx a_{1g}$ and $\alpha_{\rho\sigma} \approx \alpha_{xx,xy,xz,yx,yy,yz,zx,zy,zz}$

Thus the transition **i->f** is allowed if $\Gamma(\Psi^f_{vib}) = \Gamma(\mathbf{x^2, y^2, z^2, xz, yz, xy})$

Let us illustrate this with the example of CO_2. From Group theory, we know that CO_2 belongs to the point group $D_{\infty h}$. Hence according to the above discussion, a_{1g} normal mode of vibration is Raman active, i.e., the symmetric stretch which occurs at 1388 cm^{-1} [18]. However this band is split into two bands because of Fermi resonance with the first overtone of the doubly degenerate bending mode at 667 cm^{-1}.

B. Relation between Raman band shapes and Intermolecular potential:[19), 20)]

In Raman spectroscopy, intensity and polarization measurements of the scattered radiation give information about the polarizability of the system. Frequency measurements at low pressures furnishes information about identity of molecular systems whereas line widths, frequency shifts and bandwidth measurements provide information about the intermolecular forces. Traditionally, virial coefficients, transport properties and crystal structure have been used to provide information about isotropic forces. However transport phenomenon in polyatomic gases and molecular structures can also provide information about anisotropic forces.

For modeling Raman band shapes in SCFs, it is important to consider the regime in which one is interested. For gases, at low densities all the collision effects are negligible. Hence an isolated Raman line appears as its natural width superimposed on the Doppler width. As the density increases, the collisions increase proportionally and there is a narrowing of the Doppler lines. At higher densities, collision broadening takes over, the line width increases with gas density and line mixing occurs as a result of overlap of several broadened lines. At even higher densities, the band spectrum shows collisional narrowing.

For dense gases and liquids, we obtain mostly overlapping lines. Band moments and correlation functions are determined using molecular dynamics of such systems. The Fourier Transform of the correlation

function gives us the theoretical spectra, which can be compared with the experimental results to obtain the correct model.

Modeling Gases:

For a system in which the thermal bath consists of the foreign atoms and molecules. The Hamiltonian, **H** of the system is:

$$\mathbf{H} = \mathbf{H_0}^{(system)} + \mathbf{H_0}^{(Bath)} + \mathbf{V}$$

Where $\mathbf{H_0}^{(system)}$ **and** $\mathbf{H_0}^{(Bath)}$ are the unperturbed Hamiltonians of the system (scattering molecule) and the bath(perturbers), respectively and **V** contains all the intermolecular interactions(bath-system and bath-bath). The system correlations are neglected.

Application of the Liouville's operator L : $\mathbf{LX} = [\mathbf{H}, \mathbf{X}]/h'$ where **X** is any operator, $h' = h/2\pi$ where h is Plancks constant and **H** is the Hamiltonian of the system gives:

$$\mathbf{L} = \mathbf{L_0}^{(system)} + \mathbf{L_0}^{(Bath)} + \mathbf{L_1} \textbf{ where } \mathbf{L_1X} = [\mathbf{V}, \mathbf{X}]/\,\boldsymbol{h}'$$

The operators $\mathbf{L_0}^{(system)}$ and $\mathbf{L_0}^{(Bath)}$ are diagonal in the unperturbed system and bath states respectively. With the assumption that there is no initial correlation between the system and bath molecules, one can write the density matrix of the sample gas as a product of the density matrices of the system and bath molecules. This assumption allows one to separate, at least formally, the bath variables and write the trace only over the system variables, provided one also assumes that the distribution of bath molecules among the eigenstates of $\mathbf{H_0}^{(Bath)}$ is constant in time.

Thus one can derive the spectral function as:

$$F(\omega) = -\pi^{-1}\mathrm{Im}\ \mathbf{Tr_s}\{\underline{\underline{\alpha}}(0)[\omega - L_o^{(System)} - \mathbf{R}(\omega)]^{-1}\rho^{(s)}\underline{\underline{\alpha}}(0)\} \quad (\mathbf{B.1})$$

where $\mathbf{Tr_s}$ stands for the trace over the system variables and $\mathbf{R}(\omega)$ for the relaxation operator(matrix) which is averaged over the bath variables.

$$\mathbf{R}(\omega) = \mathrm{Tr}_b\{\rho^{(b)}R(\omega)\}. \quad (\mathbf{B.2})$$

The relaxation operator, $\mathbf{R}(\omega)$ is an operator with respect to the system coordinates. It is determined by the interaction, V or L_1, and contains information about the dynamics of the system molecule and includes many-body collisions and memory effects. It is useful to realize that the spectral function F (ω) becomes the spectral function of a non resonant Raman scattering for $\mathbf{R}(\omega) = 0$, i.e. when there are no interactions except the system and radiation.

Using the Impact Theory of collisions and assuming τ_d (the average duration of a collision) is small compared to the characteristic time of the relevant radiative process i.e. scattering of light, **R** is linear in the density of perturbers, N and its ω dependence is negligible. In such a case, **R** can be expressed in terms of S, the semi-classical two-body scattering matrix as follows:

$$\mathbf{R}_{ab,\,cd} = -i2\pi N \int_0^\infty dv\, vf(v) \sum_a \rho_a \int_0^\infty db\, b < a\,|[\delta_{ac}\delta_{bd} - \langle a|S(b)|c\rangle\langle b|S(b)|d\rangle^*]|a> \qquad \textbf{(B.3)}$$

where v is the relative velocity of the colliding molecules, f(v) is the Boltzmann velocity distribution function, N is the density of the perturber and b is the impact parameter. The internal states |a> and |b>(or |c> and |d>) are the initial and final radiative states of the system connected by the operator $\underline{\underline{\alpha}}$, whereas |a> denote an internal state of the perturber.

Thus the impact theory result for the spectral function is given by:

$$F(\omega) = -\pi^{-1}\,\mathrm{Im}\,\left\{\sum_{ab,\,cd} \langle c|\,\underline{\underline{\alpha}}(0)|d\rangle^* [\omega - L_o^{(s)} - \mathbf{R}]^{-1}_{ab,\,cd}\, \rho_a^{(s)} \langle a|\underline{\underline{\alpha}}(0)|b\rangle\right\} \qquad \textbf{(B.4)}$$

This expression is valid for both isolated and overlapping lines. In the case of isolated lines, the collisions do not mix different transitions. Therefore the overall spectrum consists of a superposition of Lorentzians without any interference. That is: $\mathbf{R}_{cd,\,ab} = \mathbf{R}_{ab}\delta_{ca}\delta_{db}$ and this reduces the spectral function to:

$$F(\omega) = -\pi^{-1}\,\mathrm{Im}\,\left\{\sum_{ab} [\omega - \omega_{ab} - \mathbf{R_{ab}}]^{-1}\, \rho_a^{(s)}\, |\langle a|\underline{\underline{\alpha}}(0)|b\rangle|^2\right\} \qquad \textbf{(B.5)}$$

where the Real and Imaginary part of $\mathbf{R_{ab}}$ determine, respectively, the shift and the width of the line $|a\rangle \rightarrow |b\rangle$. The general case of overlapping lines is quite complicated because of the $[\omega - L_o^{(s)} - \mathbf{R}]^{-1}$ term.

Assuming a rotationally invariant form of the Hamiltonian, one can write the rotationally invariant form as:

$$F(\omega) = -\pi^{-1} \mathrm{Im}\{\sum_{kabcd} \langle uc||\underline{\underline{\alpha}}^{(k)}(0)||vd\rangle^* [\omega - L_o^{(s)} - \mathbf{R}^{(k)}]^{-1}_{ucvd,uavd} \rho_a^{(s)} \langle ua||\underline{\underline{\alpha}}^{(k)}(0)||vb\rangle\} \quad \textbf{(B.6)}$$

where the polarizability tensor $\underline{\underline{\alpha}}^{(k)}(0)$ has been resolved into its irreducible components of rank k, $\langle ua||\underline{\underline{\alpha}}^{(k)}(0)||vb\rangle$ represents the reduced matrix element. Since no overlapping of vibrational bands is expected, only the matrix elements of $\mathbf{R}$ with u* = u and v* = v appear in $F(\omega)$ above. Also there is no interference between the spectrum obtained from the different irreducible components of $\underline{\underline{\alpha}}$. For Raman scattering the allowed values of k are 0, 1, 2. The k = 0 component gives the isotropic scattering and the k = 2 gives the anisotropic scattering. Due to the impact theory of collisions $|\omega - \omega_{ab}|^{-1} >> \tau_d$, $\mathbf{R}^{(k)}$ in eqn (B.5) is independent of ω.

Thus the isolated line widths have Lorentzian shapes and their widths (Half Widths at half maxima) and shifts (in wavenumber units) are:

$$\gamma_{ab}^{(k)} = -(2\pi c)^{-1} \mathrm{Im}\{\mathbf{R_{ab}}^{(k)}\}$$

and

$$\Delta_{ab}^{(k)} = (2\pi c)^{-1} \mathrm{Re}\{\mathbf{R_{ab}}^{(k)}\}$$

respectively where c is the speed of light.

The calculation of the relaxation matrix $\mathbf{R_{ab}}$ above requires calculation of the semiclassical S-matrix given by:

$$S(b) = T \exp[-i/h \int_{-\infty}^{\infty} dt\, V_I(b, t)]$$

where T is the Dyson time-ordering operator and $V_I(b, t)$ is the interaction representation of the semi-classical potential evaluated along a classical

trajectory. In general, the exact evaluation of the S-matrix is difficult. Hence several approximate methods are used.

For calculating long range potentials, perturbative approaches are used and for short-range potentials, non-perturbative approach is used. The non-perturbative approaches have been used by Smith and Giraud[21] to analyze rotational line widths in HCl perturbed by Ar. In the perturbative approaches, the S-matrix is evaluated up to 2nd order and the classical trajectory is approximated by a straight line path. The line shift is determined by the imaginary part of the S-matrix. Also, since the line-shifts are more sensitive to the short-range isotropic part of the intermolecular potential compared with the line widths, a combined investigation of the line-widths and shifts can provide more complete information about the potentials.

For H_2 perturbed by He, Shafer and Gordon[22] computed the S-matrix quantum mechanically and the results were compared to the relevant data on Raman line widths and shifts. They concluded a potential, which agreed with the experimental data as well as with the theoretical calculations of the interaction:

$V(\mathbf{r}) = V_0(r) + V_2(r)P_2(\cos\theta) = \sum_{i=0,2} V_i(\mathbf{r})\, P_i(\cos\theta)$

where

$$V_i(\mathbf{r}) = \begin{cases} \varepsilon A_i\{\exp[2\beta(1 - r/r_m)] - 2\gamma_I \exp[\beta(1 - r/r_m)]\} & , \; r \le r_1 \\ \sum^{3}_{n=0} a_n r^n & r_1 \le r \le r_2 \\ -B_I\left(c_8/r^8 + c_6/r^6 \right) & r_1 \ge r_2 \end{cases}$$

The values of all the parameters are in the reference[22].

Modeling Liquids and dense gases:[24)]

The present knowledge of liquids is rather limited and the immediate task facing the researchers is to understand the structure, molecular dynamics, and other basic properties of liquids. Most of these properties in turn are related to the intermolecular forces. The Raman spectrum of molecules in liquids usually consists of bands of overlapping lines; only for light molecules like H_2 – HD etc., are the individual lines resolved. The spectrum of pure molecular liquids involves further complications because of the correlation effects. Therefore, the spectrum of a dilute molecular solution, in a solvent of different species, generally gives more information about molecular dynamics. Raman band narrowing has been studied to provide useful information in liquids[23)]. For Liquids and dense gases, one has to apply Molecular dynamics calculations inorder to obtain information about intermolecular potentials through the correlation functions as suggested by Gordon[19)].

According to the Heisenberg picture of spectroscopy, a Raman band shape (observed by inelastic light scattering) is the Fourier transform of the average motion of the motion of the polarisability tensor of a molecule. Specifically, the *depolarized (isotropic)* component of the ro-vibrational Raman band is given by:

$$\mathbf{I_{vib}(\omega) = I_{\parallel} - 4/3\ I_{\perp} = FT(\langle Q(0).Q(t)\rangle)}$$

where **Q** is the vibrational matrix element of the polarizability anisotropy. FT denotes the Fourier Transform operator:

$$FT\ (\mathbf{x}\ (\mathbf{t})) = \int^{\infty}_{0}\ \exp\ (i\omega t)\mathbf{x(t)}\ dt$$

The *anisotropic (polarized)* part of the spectrum is similarly given by:

$$\mathbf{I_{\perp}(\omega) = FT\ (Tr(\langle \beta^{v}(0).\beta^{v}(t)\rangle)\langle Q(0).Q(t)\rangle)}$$

where β^{v} is the vibrational part of the matrix element of the anisotropy of the polarizability, taken between the two vibrational states involved in the transition. In case of linear CO_2, the correlation function **<Q(0).Q(t)>** has the form **$(1/2)\langle 3[u(0)u(t)]^2 - 1\rangle$**, where **u** is the unit vector along the axis of the molecule.

This way it is possible to separate the reorientational part **$Tr\langle \beta^{v}(0).\beta^{v}(t)\rangle$** from the vibrational relaxation part **<Q(0).Q(t)>**. This provides an indirect snapshot of the intermolecular potential, which is a part of the Hamiltonian of the system and is manifested in the correlation function.

For the case of pure dephasing and neglecting the effects of resonant transfer, population relaxation and vibration-rotation coupling, the Raman band line shape can be related to the solvent-induced modulations of the solute's vibration levels:

$$\mathbf{\Omega(t) = V_1(t) - V_0(t)}$$

This time dependant shift of the vibrational frequency relative to the gas-phase frequency ω_0 arises from the difference in the solute-solvent interactions ("V") when the solute is in its $\nu = 1$ and $\nu = 0$ vibrational levels. **$\Omega(t)$** is related to **<Q (0)|Q(t)>** through an integral. The line shape is related to fluctuations about the average $\langle\Omega\rangle$ via $\delta\Omega(t) = \Omega(t) - \langle\Omega\rangle$ through the autocorrelation function: $\langle\delta\Omega(0)|\delta\Omega(t)\rangle$. The intermolecular potentials are in thus $\Omega(t)$ e.g., expansions about **Q = 0** for a ground state

model or a dispersion model depending on the appropriate environment under consideration.

To summarize, Raman spectrum studies in liquids have been used to provide information using molecular dynamics. However, reliable quantitative theories for the measured quantities e.g., relaxation times and diffusion constants in terms of intermolecular forces are not fully developed. Hence attempts are being made in this direction to provide more fully developed information.

III. EXPERIMENTAL SETUP AND MEASUREMENT:

A. Design of High P, High T laser Raman spectroscopic system:

Fig. 3 shows an outline of the experimental arrangement of the high P, high T laser Raman spectroscopic system. The Raman Jasco Model# NR 1000, which includes the monochromator, the Ar+ laser (514.5nm) and the data acquisition station, was generously shipped to us from Asahi chemicals. Liquid CO_2 (dry bone grade, 99.8% purity) cylinder was obtained from BOC gases. The detector is a Photomultiplier tube. The acquired signal is collected and plotted at the data station and the signal is sent to the Virtual Bench Scope acquired from National Instruments to be plotted and saved as a text file for later analysis (for details see section on computer interface).

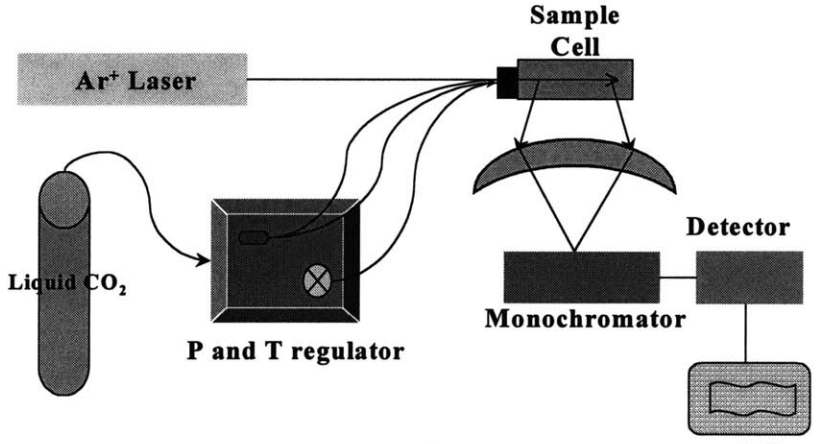

Fig.3 Outline of the experimental setup

The Raman cell as shown in Figure. 4 is made up of stainless steel and its internal volume is about 3ml. Two flat sapphire plates (each 1mm thick) are used for the windows. We designed the high T, high P Raman cell of

stainless steel such that it could withstand extremely high conditions of supercritical water i.e. T=374°C and P=218 bar.

B. Measurement procedure:

We wrapped a small heater around the cell and we were able to regulate the temperature using a small thermostat and pressure using an expansion and compression pump. The scattered light was collected perpendicular to the laser incident direction. The design of the glands as indicated in Fig.4 is schematically represented in Fig.5. With liquid CO_2, it took less than 5 minutes to reach the supercritical conditions. After adjusting the laser power to 100mW for an exposure time of 10 seconds, the light intensity was finely tuned to an optimum level and the Raman signal was obtained using methanol as a sample and then CO_2 was checked. The temperature was measured at a point, which was just under the center of the cell and received the laser light. The measured temperature was considered the cell temperature. For temperature calibration, the pressure was measured in the two-phase region, where gas and liquid coexisted at an arbitrary selected temperature and the temperature was compared with the known temperature corresponding to the saturation point according to the thermodynamic tables.

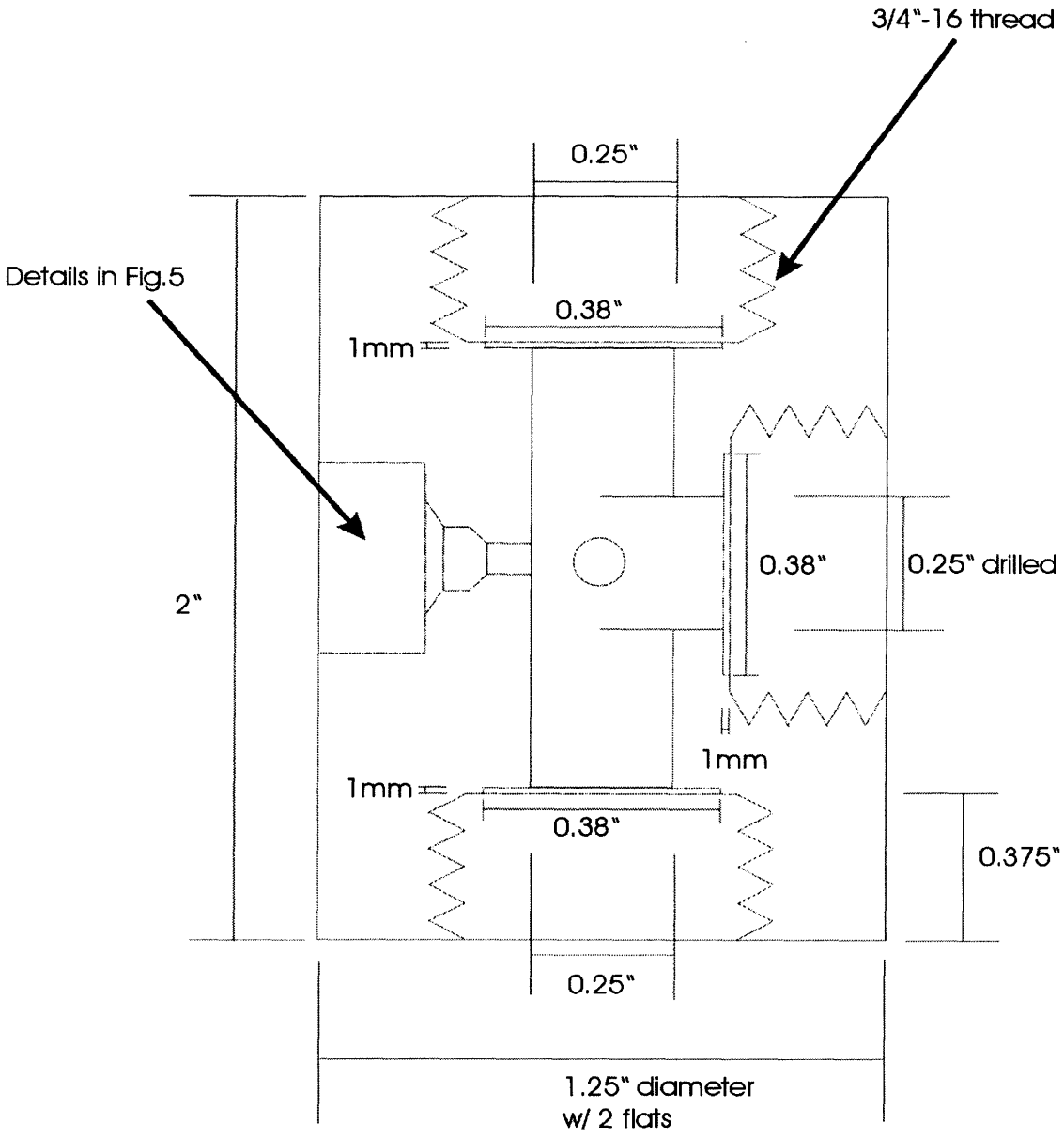

Fig.4: High T, High P Raman cell

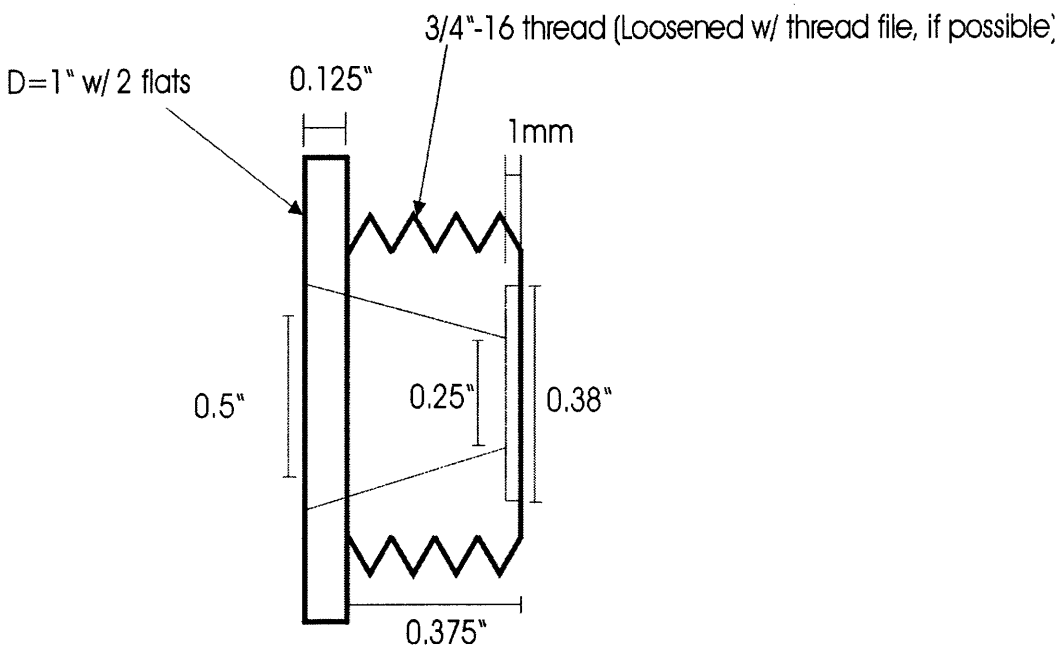

Fig. 5: Specification of the glands as seen in Fig.4

C. Computer Interface for Data Acquisition from the data station

The Computer Interface for the data acquisition from the Raman data station created problems initially because we attempted to transfer the data from the Raman data station to the computer using an **RSC232** (Remote Serial Cable) interface since there was already an A/D Card in the data station. This is a standard way of transferring data from processing stations as long as they have an A/D card. However, this procedure did not work for us, although we were told that people at Jasco were using a similar method for transferring data and storing the data on the floppy using an NEC-Basic program. In my opinion, the reason why this did not work for us is that there was no way of knowing whether the A/D Card was actually responding through a small program that I wrote in Microsoft QuickBasic even though we connected it correctly to the computer.

Also, it seemed that the computer needed some kind of a driver program to recognize the card inside the data station before it could read/write to it *(This is just a guess).* Hence, after months of frustration we had to abort the idea of retrieving data this way and we decided to contact National Instruments. National Instruments is a company in Austin, Texas and they sell and market software as well as hardware for experimental data processing. Following their recommendation, the data was transferred from the data station to the computer using **BNC** cables and a BNC-2110 connector box. The BNC-2110 connector box comes with 15 BNC connectors and a digital screw terminal with 30 pins. So, basically we connected the two channels from the data station which were previously the x and the y input for the oscilloscope to the BNC connector box. The box was connected to the computer through a 68 pin shielded cable. We also acquired a PCI-6023E card from National Instruments. PCI-6023E is a National Instruments Data acquisition (NI-DAQ) card and includes DAQ software, which provides an extensive library of functions for digital I/O boards and other devices. Thus, we basically connected the input to the oscilloscope as our input to the Data acquisition card, also acquired from National Instruments and we were able to view the signal on the Virtual Bench scope, which imitates an Oscilloscope. The virtual bench scope is a Computer interface written in labview and is user-friendly software, which includes help menus for any questions that the user might have.

The instructions on how to see the data in the VirtualBench scope are very simple. We collected data at the rate of 2000 samples/sec. Just push the RUN CTRL -> CRT keys on the data station for the data to be sent to the oscilloscope *(Refer to the Manual on NR-1000 from JASCO)* after the data acquisition and view the x-y graph after clicking the **run** icon on the left hand corner. Then when the correct graph can be seen on the screen, the user can click File followed by save waveform to save the waveform in a

text file which can be viewed in other mathematical programs or can be loaded into virtual bench scope for later visualization. *(Please refer to the documentation on Virtual Bench Scope for help).*

This way we were able to save the data in Microsoft Excel and were able to plot them according to our convenience. The BNC connection thus took only two inputs: **Ch0 as Wavenumber (in millivolts)** which was converted to **cm^{-1}** and **Ch1 as Intensity (in arbitrary units)**. It was easy to see that the output on the plotter was the same as the output on the computer screen using the Virtual Bench scope.

IV. RESULTS AND INTERPRETATION:

A. Temperature dependence of the spectrum

Fig. 6 and Fig. 7 show the spectra of the **C = O** symmetric stretch at 1280 cm^{-1} and 1385 cm^{-1}. Although the symmetric stretch of normal CO_2 occurs at 1388 cm^{-1}, it is split into 2 bands because of Fermi resonance with the first overtone of the doubly degenerate bending mode at 667 cm^{-1}. In Fig. 6, the spectra are taken at 800psi or 55 bars and at 23.8, 31.1 °C. The 2 bands at these conditions demonstrate a difference in Intensity because the Intensity is proportional to the band strength in the matrix element and since these bands arise from a linear combination of 2 wavefunctions (symmetric normal mode and a bending mode), the $|\text{linear coefficients}|^2$ are different in the two cases. Also due to a increase in temperature, the intensity decreases because the density of the system decreases from 0.877 gms/cc to 0.18 gms/cc due to a phase change (see Fig. 10) and since intensity is proportional to the number density of the scatterers, the intensity decreases proportionally. Also as a point of observation, it is clear that the width of the bands do not change at all, hence width or FWHM (Full width at Half maxima) is not a good parameter for modeling these Raman bands. Fig. 7 shows similar features. The graph of interest is at 1500 psi or 103 bars and 41.4 °C. The Supercritical conditions for CO_2 are at 31.1 °C and 74 bars, hence this is definitely in the supercritical regime. The band shapes do not change appreciably except the bands are slightly blue shifted perhaps due to a different environment, this would also seem to indicate that the environment is like a dense gas rather than a liquid. Whether any structural changes take place as a function of T are not clear from these graphs, Fig. 11 is an attempt in this direction by plotting Intensity as a function of density.

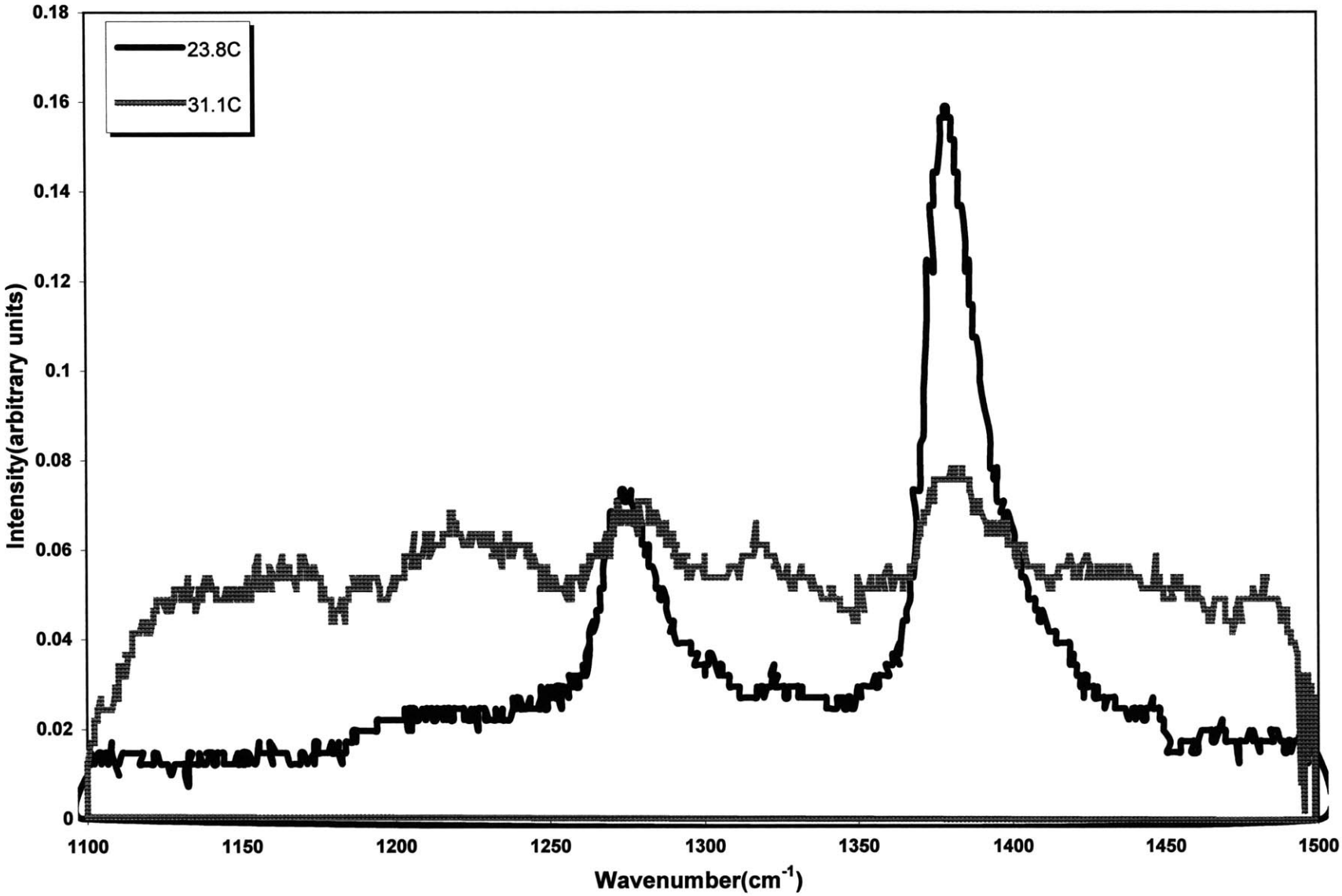

Fig. 6 Raman spectra of CO_2 at P=800 psi

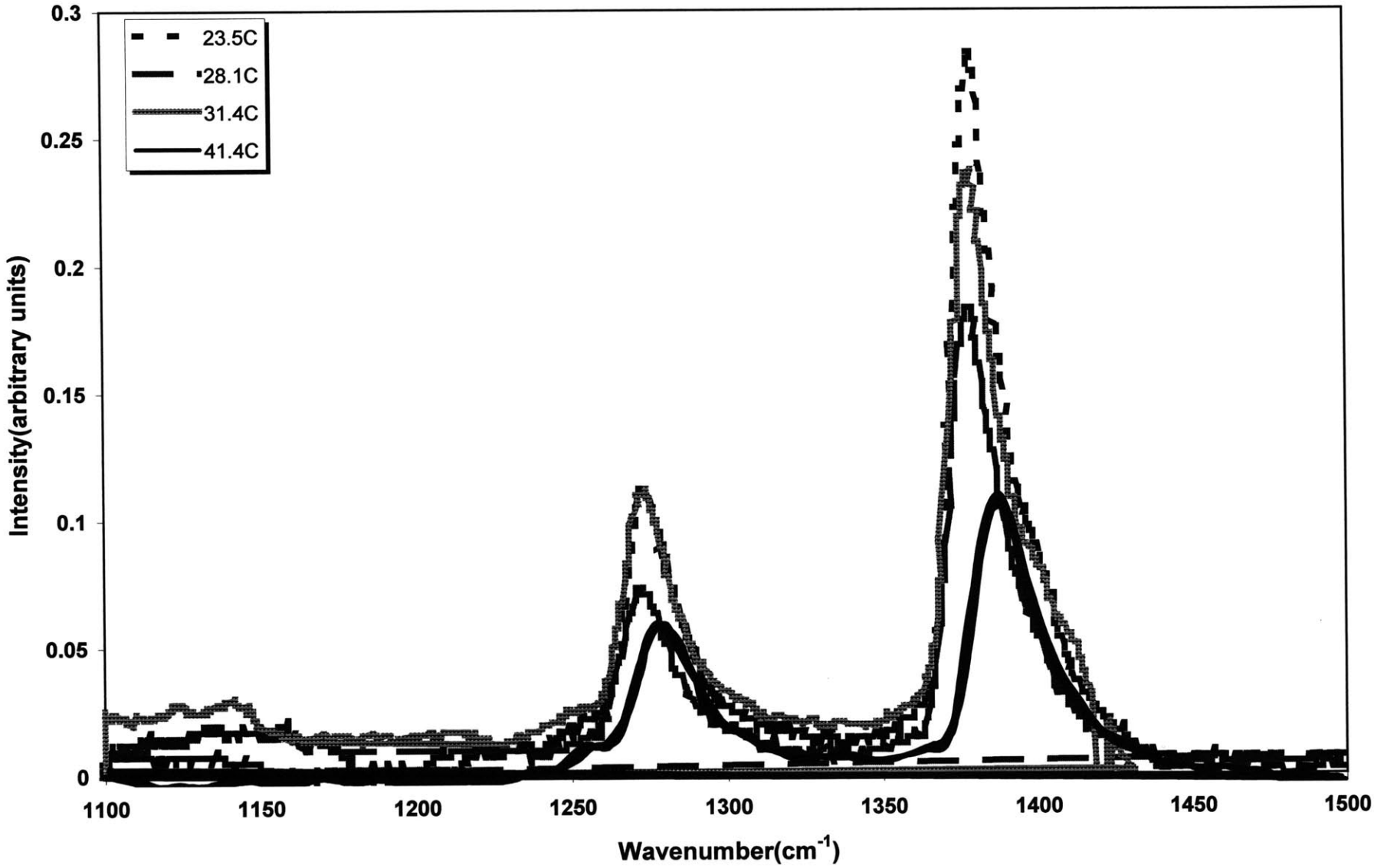

Fig. 7 Raman spectra of CO_2 at P=1500 psi

B. Pressure dependence of the spectra

The Pressure dependence of the Raman spectrum is clearly demonstrated in Fig.8 and Fig.9 where the graphs are at 23.6 °C and 800, 900, 1100 and 1500 psi or 55, 62, 75 and 103 bars respectively. In Fig.9 the conditions are 31.2 °C and 800, 1070 and 1500 psi or 55, 73 and 103 bars. Again this shows similar features in terms of the reduction in Intensity with a decrease in density, however it is clear that the reduction in density scales at a different rate for T and P respectively. Again the graphs do not show Wavenumber shifts as the T and P are increased. As pointed out earlier since the width does not change in all of these graphs, we have not considered it as a good parameter, a regression analysis of the intensity as a function of the density clearly demonstrates the model that we need for relating the Band shapes to a T and P dependence through density. A curve fitting exercise in Polynomial regression on the data in Fig. 11 shows that the curve increases in Intensity as a function of density. The supercritical density of CO_2 is 0.47 gms/cm^3. Thus the graph experimentally validates that CO_2 undergoes phase changes and changes in the surrounding environment i.e., from a liquid state to a gaseous state to a Supercritical state as a function of T and P, however a theoretical model is clearly needed to relate this. For this one needs a molecular dynamics simulation of the overall environment to get a theoretical Intensity spectra.

The Theory on how this can be done is already presented in the Section II in Theory where I have tried to explain how the Raman band shapes can be related to Intermolecular potential.

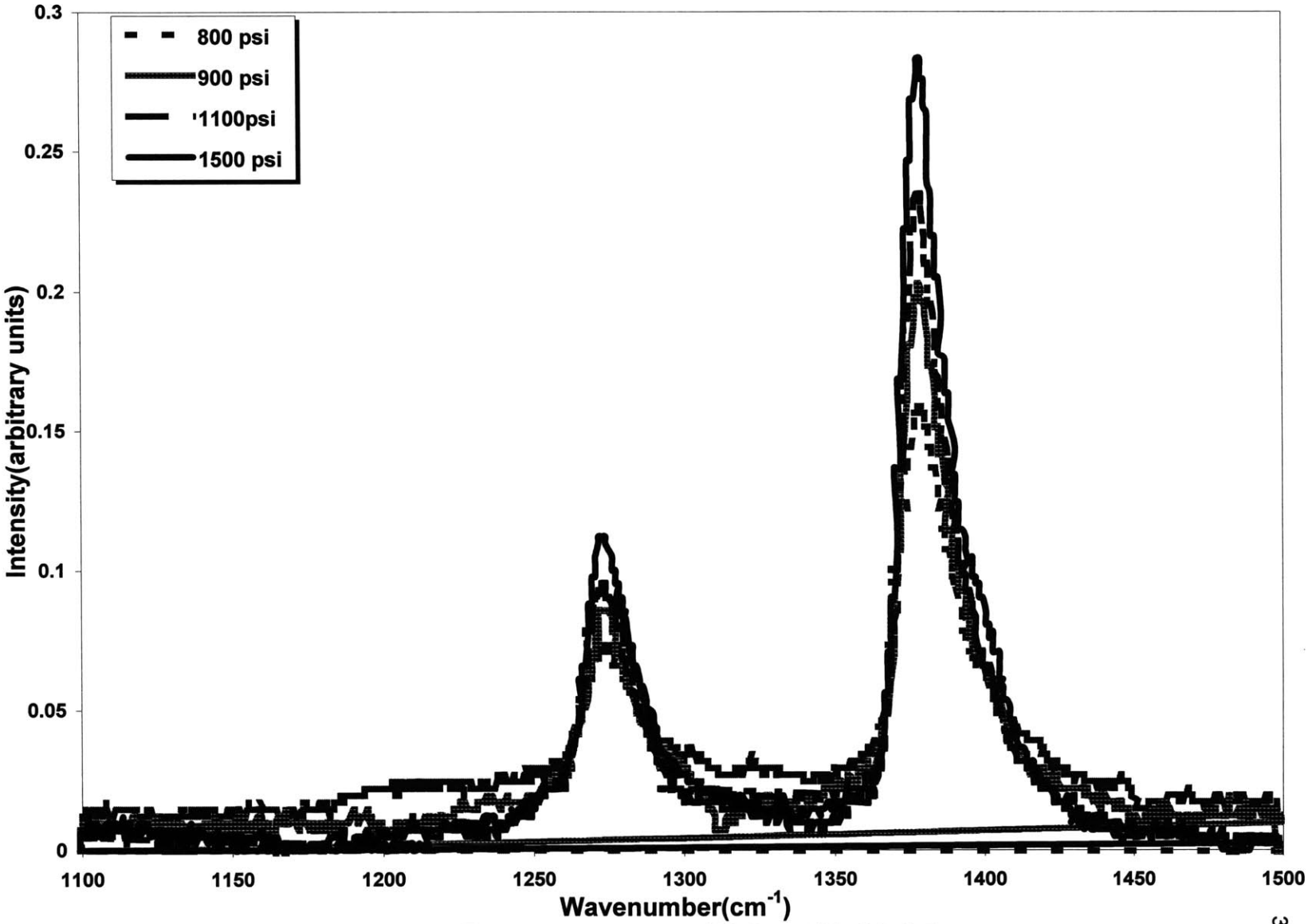

Fig. 8 Raman spectra of CO_2 at T=23.6 C

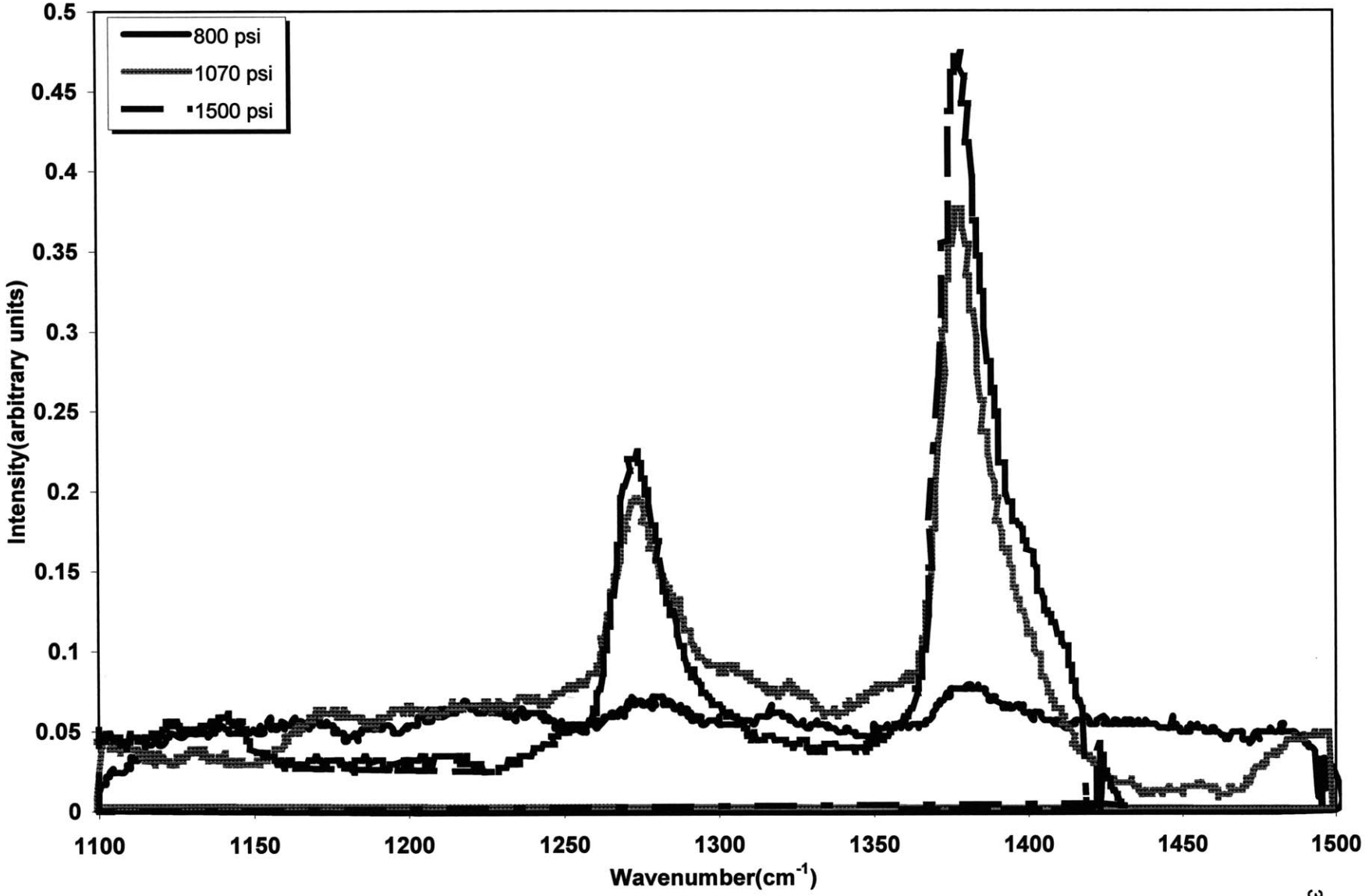

Fig. 9 Raman spectra of CO_2 at T=31.2C

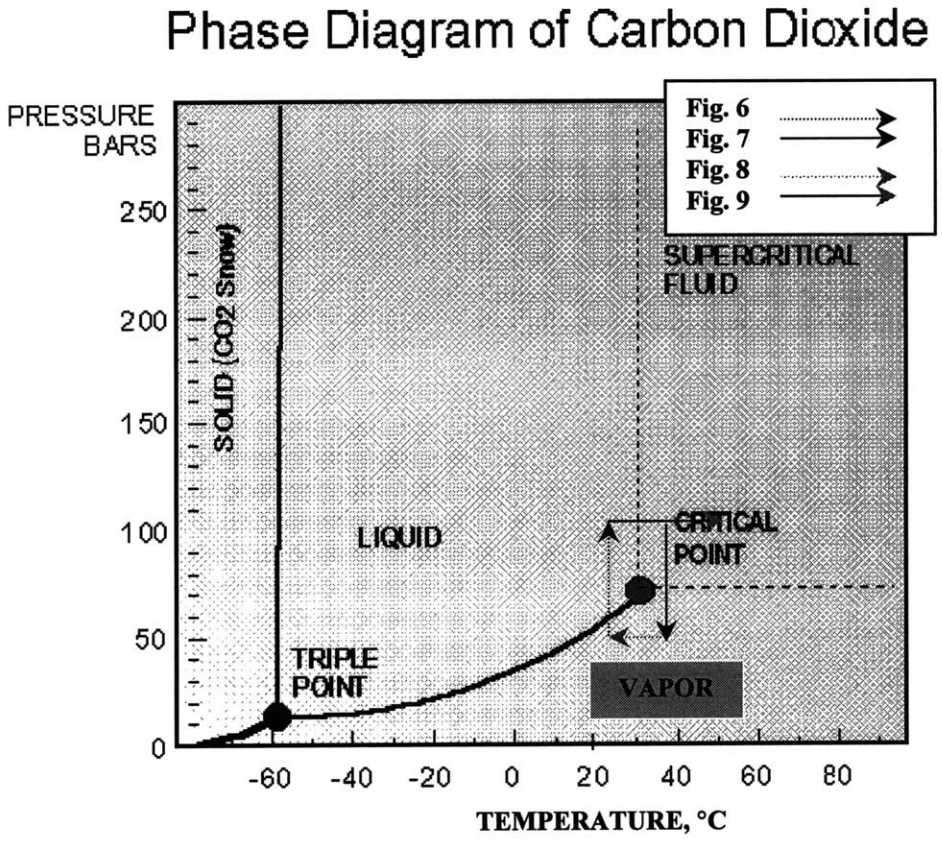

Fig. 10: Phase diagram to illustrate the phase changes in CO_2 for Raman Intensity Vs Density

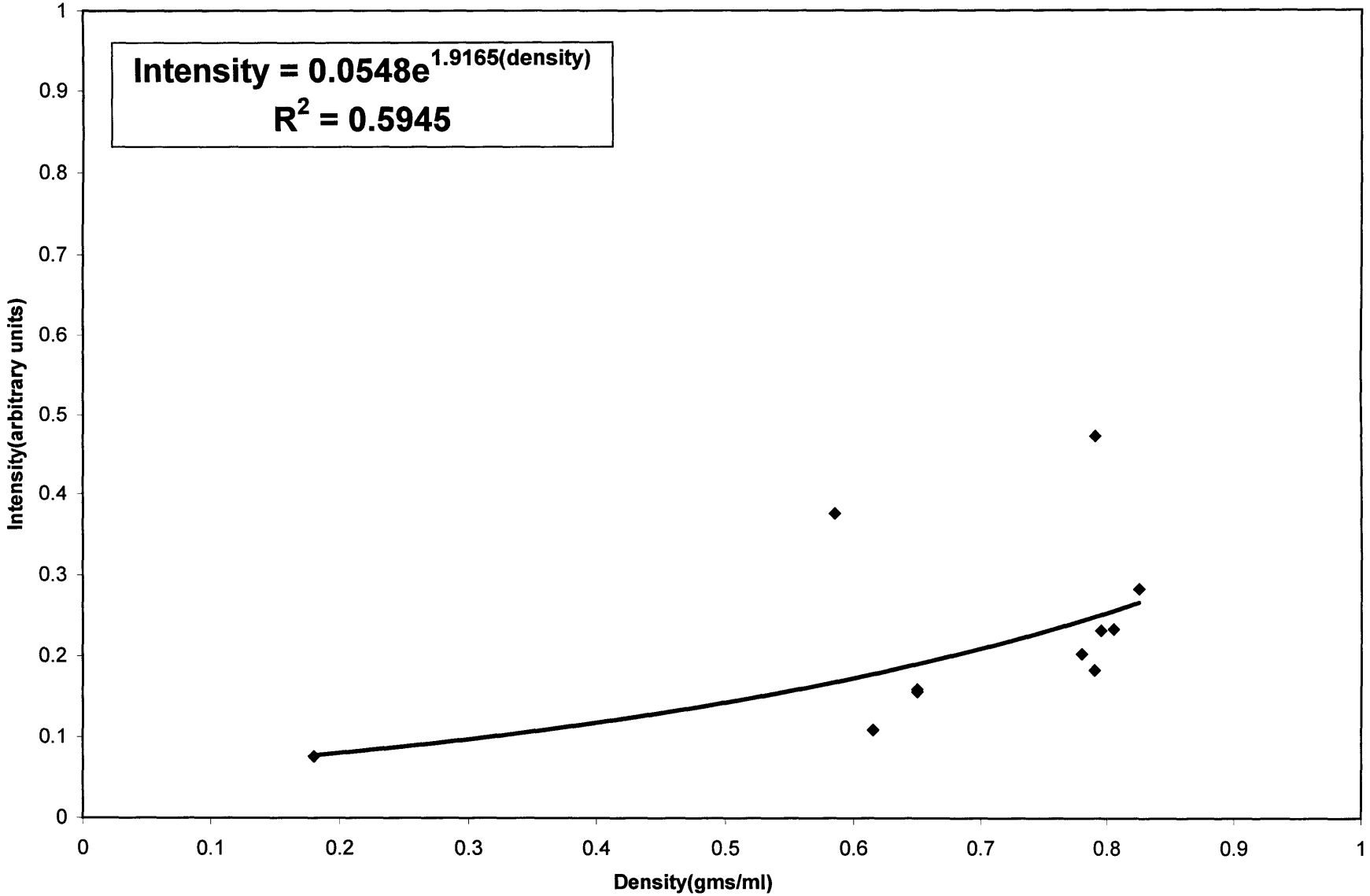

Fig. 11: Raman Intensity Vs Density for CO_2

V. CONCLUSION:

A high T, high P laser Raman spectroscopic system was used to study $SCCO_2$ at 73 bar and upto 41.4°C, focusing on the experimental process and the interpretation of the results. It is revealed that the symmetric stretch shows an increase in Intensity as a function of density. Also the dependence of Intensity to various Ts and Ps examined. A further clarification of these results involves a detailed examination of the Raman bands and establishing the correlation through molecular dynamics simulations to predict the solvation effects in $SCCO_2$. It is hoped that this study will help in studying insitu organic reactions in $SCCO_2$ and provide a suitable methodology for designing environmentally benign chemical processes.

References:

1) Howdle, S.M. and V.N.Bagratashivili : *Chem. Physics Letters*, **214**, 215(1993).
2) Akimoto, S. and Kajimoto, O. : *Chem. Phys. Letters*, **209**, 263(1993)
3) Romack, T. J., J.M.DeSimone and T.A.Treat : *Macromolecules*, **28**, 8429(1995).
4) P.E.Savage, S.Gopalan, T.I.Mizan, C.J.Martino and E.E.Brock: *AIChE J.*, **41**, 1723-1778(1995).
5) T. Xiang, K.P.Johnston : *J. Phys. Chem.*, **98**, 7915 (1994).
6) Katz, S.N., J.E.Spence, M.J.O'Brian et.al. : "*Method for Decaffeinating Coffee with a Supercritical Fluid*", **USPatent 4**, 911, 941(1990).
7) McHugh, M.A. and V.J. Krukonis, *Supercritical Fluid Extraction*, **2nd ed.**, Butterworth-Heinmann, Boston(1994).
8) Y.Ikushima, N.Saito and M.Arai: *J. Phys. Chem.*, **99,** 8941-8944(1995).
9) J.B.Ellington and J.F.Brennecke: *J. Chem. Soc. Chem. Comm.*, 1094-1095(1993).
10) Maneke, G, J. Schroeder, J. Troe and F.VoB, "*Picosecond Absorption Study of the Photoisomerization of Stilbene in Compressed Gases and Liquids.*" :*Ber. Bunsenges. Phys. Chem.*, **89**, 896-906(1985).
11) Pan, Xun, McDonald, J. C., MacPhail, R. A.: *J. Chem. Phys.*, **110**, 1677(1999).
12) Masten, D. A., B. R. Foy, D. M. Harradine and R. B. Dyer, "*In Situ Raman Spectroscopy of Reactions in Supercritical Water*": *J. Phys. Chem.*, **97,** 8557-8559(1993).
13) A.H. Narten and H.A.Levy: *J. Chem. Phys.*, **55,** 2263-2269(1971).
14) A. Adachi, H. Kiyoyama, M. Nakahara, Y. Masuda, H. Yamatera, A.Shimizu and Y. Taniguchi: *J. Chem. Phys.*, **90,** 392-399(1989).
15) Kohl, W., H.A.Lindner and E.U.Frank: *Ber Bunsenges Phys. Chem.* **95**, 1586(1991)
16) Berger, A.J., Y.Wang, D.M.Sammeth, et.al.: *Applied Spectroscopy*, **49**, 1164(1995).
17) Grasselli et. al., *Chemical Applications of Raman Spectroscopy,* Wiley-Interscience Publication(1981)
18) B. Schrader, *Raman/IR atlas of Organic compounds*(1989).
19) Gordon, R.G.;"*Molecular Motion in Infrared and Raman spectra*", *J.Chem. Phys.*, **43**, 1307(1965)
20) R. P. Srivastava and H. R. Zaidi, "*Intermolecular Forces Revealed by Raman Scattering*" in A. Weber(ed.), *Raman Spectroscopy of Gases and Liquids*, 167-201(Springer Verlag, Berlin, 1979).
21) Smith, E.W., Giraud, M.: *J. Chem. Phys.*, **66**, 1762(1977)
22) Shafer, R., Gordon, R. G.: *J.Chem. Phys.*, **58**, 5422(1973)
23) Altmann, K., Holzer, W.: *Chem. Phys. Letters*, **24**, 212(1974)
24) Frakland, S. J. and Maroncelli, M: *J. Chem. Phys*, **110**, 1687(1999)